MDCT findings of extrapancreatic nerve plexus invasion by pancreas head carcinoma: correlation with en bloc pathological specimens and diagnostic accuracy

doi: 10.1007/s00330-010-1727-5

MDCT Findings of Extrapancreatic Nerve Plexus Invasion by Pancreas Head Carcinoma: Correlation with en Bloc Pathological Specimens and Diagnostic Accuracy

Kentaro Mochizuki, MD[1], Toshifumi Gabata, MD[1], Kazuto Kozaka, MD[1], Yuki Hattori, MD[1], Yoh Zen, MD[2], Hirohisa Kitagawa, MD[3], Masato Kayahara, MD[3], Tetsuo Ohta, MD[3], Osamu Matsui MD[1]

[1]Department of Radiology, Kanazawa University Graduate School of Medical Science, Kanazawa, Japan. [2]Division of Pathology, Kanazawa University Hospital, Kanazawa, Japan. [3]Department of Gastroenterological Surgery, Kanazawa University Graduate School of Medical Science, Kanazawa, Japan.

Research institution address

Department of Radiology, Kanazawa University Graduate School of Medical Science, 13-1 Takaramachi, Kanazawa 920-8641, Japan

Tel: +81-76-265-2323

Fax: +81-76-234-4256

Correspondence address:

Kentaro Mochizuki, MD

Department of Radiology, Kanazawa University Graduate School of Medical Science, 13-1 Takaramachi, Kanazawa 920-8641, Japan

Tel: +81-76-265-2323

Fax: +81-76-234-4256

E-mail: motchii@rad.m.kanazawa-u.ac.jp

Abstract

Objective:

To elucidate the MDCT findings of extrapancreatic nerve plexus (PLX) invasion by pancreas head carcinoma (PhC) by “point-by-point” correlation with en bloc pathological specimens and to assess their diagnostic accuracy.

Methods:

Each pathological section of PhC and adjusted double oblique multiplanar reconstruction MDCT images were correlated in 554 sections from 37 patients. The diagnostic accuracy of the MDCT patterns derived was assessed by blind reading.

Results:

PLX invasion with fibrosis showed mass or strand shape (85.6%) or coarse reticula (13.3%). The CT findings were divided into fine reticular and linear, coarse reticular, mass and strand and nodular patterns. PLX invasion was revealed pathologically in 92% of the

regions of investigation showing the mass and strand pattern and 63% the coarse reticular pattern (all continuous with PhC), and they were highly suggestive of PLX invasion by PhC on MDCT images ($p < 0.001$). Sensitivity, specificity, accuracy, and positive and negative predictive values of these MDCT findings in the diagnosis of PLX invasion were 100% (25/25), 83.3% (10/12), 94.6% (35/37), 92.6% (25/27) and 100% (10/10), respectively.

Conclusion:

The mass and strand pattern and the coarse reticular pattern continuous with PhC on MDCT images were highly suggestive of PLX invasion by PhC.

Introduction

Pancreatic carcinoma still has a poor prognosis [1; 2]. Only surgical resection has the potential to be curative [3]. For pancreas head carcinoma (PhC), when potentially curative resection is achieved, the 5-year survival rate is approximately 10-20% [1; 3; 4]. Extrapancreatic nerve plexus (PLX) invasion is one of the most important prognostic factors in patients with PhC, and therefore, preoperative imaging diagnosis of PLX invasion in PhC is clinically important for predicting the prognosis and deciding the surgical strategy including extended resection with removal of the adjacent major vessels [5-14].

Recently, the spreading patterns of PLX invasion in PhC have been investigated in detail pathologically [12; 15]. However, few reports have focused on the imaging findings of PLX invasion in PhC [16-19]. Furthermore, these past reports were not sufficiently accurate, because a point-by-point correlation between the images and pathological findings was not performed.

In this study, to make point-by-point imaging-pathological correlation possible, we cut the surgical specimens of PhC resected en bloc with the surrounding vessels, lymph nodes and connective tissues including PLX horizontally, and made double oblique multiplanar reconstruction (MPR) images from multi-detector row computed

tomography (MDCT) that were exactly equal to each of the pathological sections. The purpose of this study was to elucidate the MDCT findings of PLX invasion by PhC by “point-by-point” correlation with en bloc pathological specimens and to assess the diagnostic accuracy of the MDCT findings in the diagnosis of PLX invasion.

Materials and methods

Our institutional review board approved this retrospective study and informed consent was obtained from each of the patients.

Study Design

First, we performed “point-by-point” correlation between the MDCT findings and pathological specimen at the same section to clarify the MDCT findings of PLX invasion. Then, from this analysis, the representative MDCT patterns indicating the presence/absence of PLX invasion were derived. Last, we determined the diagnostic accuracy of these MDCT patterns in the diagnosis of PLX invasion by blind assessment by experienced radiologists.

Patients

Thirty-seven consecutive patients with invasive ductal carcinoma of the pancreas head who received preoperative MDCT examination and en bloc curative surgical resection within one month during the period from January 2003 to June 2007 at our institution were focused on in the study. Thirteen female (mean age, 63 years; age range, 52-74 years) and 24 male (mean age, 62 years; age range, 44-79 years) patients were included. Thirty-three patients had tubular adenocarcinomas, and four had adenosquamous carcinomas. None of the patients received preoperative chemotherapy, radiation, or other neo-adjuvant therapy. En bloc resection of PhC, peripancreatic adipose tissue including regional PLX, lymph nodes and duodenum was performed in all patients. Combined resection of the proximal portion of the portal vein (PV) was performed in 16 patients, and both the superior mesenteric artery (SMA) and PV in 16 patients. The mean size and size range of the tumours were 3.1cm and 1.7-4.5cm, respectively. PLX invasion was revealed in 25 patients pathologically.

Surgical specimens and pathological sections

Resected specimens were immediately fixed in 10% buffered formaldehyde solution. After the specimens were cut in a transverse plane of the body approximately parallel to axial CT sections into 5 mm stepwise tissue blocks, they were embedded in paraffin. The 5 μm

sections were cut for haematoxylin and eosin (H&E) and Elastica van Gieson (EVG) staining, and full mount preparations were created. We obtained a total of 554 pathological sections. The mean number of created pathological sections per patients was 15.

CT examinations and MPR images

CT examinations were performed using a 16 (29 patients) or 4 (8 patients) –detector row CT (LightSpeed Ultra, LightSpeed Plus; GE Medical Systems, Milwaukee, WI, USA). Images were acquired through the pancreas in a craniocaudal direction with 0.562:1 (16-detector), 0.75:1 (4-detector) pitch. Other CT parameters were the same in both systems, as follows: 300-350 mA; 120 kV; gantry rotation speed, 0.5 s; a reconstruction section thickness of 1.25 mm and a reconstruction interval of 1.25 mm. Unenhanced multi-detector row CT was performed first. For dynamic CT, contrast medium with a concentration of 300 mg of iodine per millilitre (Omnipaque, Daiichi, Tokyo, Japan) was administered with a power injector. A total volume of 100 ml was injected at a rate of 3 ml/s through a 22-gauge plastic intravenous catheter that was placed in an antecubital vein. Three-phase (35, 60, 180 seconds after initiation of the injection) CT acquisition was performed. This is the routine protocol for upper abdominal CT examination at our institution.

After reviewing all pathological sections, double oblique MPR for both the ventrodorsal and lateral directions were generated with a slice thickness of 2.5mm and reconstruction intervals of 1.0mm from the first phase data set using a workstation (Virtual Place Lexus 1.0, AZE, Tokyo, Japan). Double oblique MPR images were precisely coordinated equal to the parallel section of the pathological sections referring to the configuration of the pancreas or tumour and to the surrounding vessels such as the gastroduodenal artery, pancreaticoduodenal arteries and PV and its branches, bile duct, and lymph nodes by two authors (K.M., K.K., both with 9 years' experience in abdominal radiology) by consensus. We obtained a total of 554 sectional MPR images exactly equal to the number of pathological sections.

CT images were reviewed using window level 40 and window width 350, and using the same monitor in this study.

Correlation between CT and pathological findings

The region of investigation was determined according to the anatomy of PLX related to PhC invasion described in previous reports [15; 20; 21] as shown in Fig. 1. It was the medial-posterior fat area of the pancreas head surrounded by the parenchyma of the pancreas, PV, common hepatic artery, a median line connecting PV and inferior vena

cava, a median line connecting the SMA and aorta, a median line connecting the celiac artery and aorta, and anterior border line connecting the aorta and inferior vena cava.

All pathological sections were reviewed by two authors (Z.Y., with 10 years' experience in pathology and K.M.) and all pathological structures more than 1mm in these regions were recorded. Then the point-by-point correlation between the pathological and CT findings was carried out by two radiologists (K.M., K.K.) and one pathologist (Z.Y.) by consensus with careful comparison of the exactly the same sections of the MPR images and surgical specimens.

Deriving CT patterns and correlation between each pattern and pathological findings

According to the above mentioned correlation analysis, the CT findings in the region of investigation were classified into several representative patterns with special reference to PLX invasion.

Then, two radiologists (K.M., K.K.) reviewed all sections of MPR images in all patients and classified the CT findings of each evaluated area into these patterns by consensus. These patterns and pathological findings were then correlated to extract the particular CT patterns reflecting PLX invasion. When the same pattern was observed continuously in two or more consecutive sections, it was counted as

one evaluation area of this particular pattern. As a result, a total of 276 evaluation areas were extracted.

Evaluation of the diagnostic accuracy of MDCT findings

Two independent radiologists (reader A; Y.H., and reader B; T.G., with 10 and 26 years' experience in abdominal radiology, respectively) had been informed of the definitions of each CT pattern and CT patterns reflecting or not reflecting PLX invasion by using cases not included in this study. For evaluating the diagnostic accuracy of the CT patterns in the diagnosis of PLX invasion, the two readers independently reviewed the routine CT images of all patients and diagnosed the presence or absence of PLX invasion in each. The readers were blinded to the patient pathological information.

For analysing interobserver variability, two readers (Y.H., T.G.) independently reviewed all the MPR images and classified the CT findings of 276 evaluation areas into derived CT patterns.

Statistical Analysis

The statistical analysis was performed using Statistical software (SPSS for Windows; SPSS, Chicago, IL, USA). P values less than 0.05 were considered statistically significant.

After taking into account the presence or absence of the

continuity of each pattern, for evaluating the correlation between PLX invasion and each pattern, pattern-by-pattern basis cross-tabulation tables were prepared and a chi-squared test was carried out.

For evaluating the diagnostic accuracy of the CT patterns in the diagnosis of PLX invasion by two readers, two patient-by-patient basis cross-tabulation tables were prepared and the sensitivity, specificity, accuracy, and positive and negative predictive values were calculated for each table.

To assess interobserver variability in terms of image interpretation, k statistics was used to quantify the degree of agreement. A k value of up to 0.20 was considered to indicate slight agreement; a k value of 0.21-0.40, fair agreement; a k value of 0.41-0.60, moderate agreement; a k value of 0.61-0.80, substantial agreement; and a k value of 0.81 or greater, almost perfect agreement.

Results

Correlation between CT and pathological findings

Among all 554 pathological sections in all 37 patients, we identified 268 micro-vessels, 14 fibrotic thickenings of adipose tissue septa, 133 clusters of micro-vessels with fibrotic thickening of adipose tissue septa, 175 lymph nodes, 90 cases of PLX invasion with fibrosis

and 4 cases of inflammatory cell infiltration. All cases of PLX invasion with fibrosis were continuous with PhC (90/90, 100%).

On MPR images, all of the micro-vessels showed fine lines (less than 2mm in diameter) (268/268, 100.0%) (Fig. 2). All fibrotic thickenings of adipose tissue septa also showed fine lines (14/14, 100.0%). Clusters of micro-vessels with fibrotic thickening of adipose tissue septa showed fine reticula (reticulation that was composed of fine reticular lines with abundant intermingled fat density) (127/133, 95.5%) (Fig. 3) or coarse reticula (reticulation that was also composed of reticular lines with less intermingled fat density) (6/133, 4.5%). Lymph nodes (with or without metastasis) showed fine lines (59/175, 33.7%) or mass or strand shape (over 2mm diameter mass or strand-shaped soft tissue density continuous with PhC (6/175, 3.4%), or nodules (over 2mm diameter isolated nodules) (110/175, 62.9%) (Fig. 3). PLX invasion with fibrosis showed mass or strand shape (77/90, 85.6%) (Fig. 4) or coarse reticula (12/90, 13.3%) (Figs. 3, 4) or fine reticula (1/90, 1.1%). All inflammatory cell infiltrations showed coarse reticula (4/4, 100%) (Fig. 5).

Deriving CT patterns and correlation between each pattern and pathological findings

According to this correlation analysis, considering the presence

or absence of PLX invasion, the CT findings of the investigated regions were divided into the following four categories (Fig. 6):

a. Fine reticular and linear pattern: fine lines (less than 2mm in diameter) and fine reticula (reticulation that was composed of fine reticular lines with abundant intermingled fat density).
b. Coarse reticular pattern: coarse reticula (reticulation that was also composed of reticular lines with less intermingled fat density).
c. Mass and strand pattern: over 2mm diameter mass or strand-shaped soft tissue density connecting to the PhC.
d. Nodular pattern: over 2mm diameter isolated nodules.

Table 1 shows the numbers of the areas showing each CT pattern and the corresponding pathological findings.

Fine reticular and linear pattern: 113 areas showing a fine reticular and linear pattern were detected on the MPR images in 35 patients. 112 (99%) of them showed micro-vessels, micro-lymph nodes and fibrosis with PLX (Figs. 2, 3). The remaining one (1%) of them, which was continuous with PhC, showed PLX invasion by a small number of cancer cells with fibrosis (Fig. 7).

Coarse reticular pattern: 43 areas showing a coarse reticular pattern were detected on the MPR images in 20 patients. 16 (37%) of

them showed clusters of micro-vessels, micro-lymph nodes, and fibrosis with PLX, similar to those observed in the fine reticular and linear pattern. Inflammatory cell infiltration was mixed in two of these 16 areas (Fig. 5). PLX invasion with fibrosis was observed in 27 areas (63%) (Fig. 4). All areas with PLX invasion were continuous with PhC. On the other hand, 9 areas without PLX invasion were also continuous with PhC.

Mass and Strand pattern: 25 areas showing a mass and strand pattern were detected on the MPR images in 22 patients. 23 (92%) of them showed PLX invasion with fibrosis (Fig. 4). The remaining two (8%) showed lymph nodes attached to PhC. Metastatic tumour cells were not identified in these lymph nodes.

Nodular pattern: 95 areas showing a nodular pattern were detected on the MPR images in 28 patients. All of them showed lymph nodes (Fig. 3), with 14 (15%) of them showing metastasis and 81 (85%) of them no metastasis.

As a result, when we regarded a coarse reticular pattern continuous with PhC and a mass and strand pattern as reflecting PLX invasion and the other patterns as not reflecting PLX invasion, a significant statistical difference was noted between the two ($P < 0.001$).

Evaluation of the diagnostic accuracy of MDCT findings

Two patient-by-patient basis cross-tabulation tables about MDCT diagnosis and the pathological result of PLX invasion were prepared by two readers (Table 2). These two tables were similar, and sensitivity, specificity, accuracy, and positive and negative predictive values were 100% (25/25), 83.3% (10/12), 94.6% (35/37), 92.6% (25/27) and 100% (10/10), respectively. The k values of independent image ratings by readers A and B for the CT classification was 0.88, indicating substantial, almost perfect agreement.

Discussion

Only a few previous reports have focused on the imaging findings of PLX invasion in PhC [16-19]. This may be due to the complicated anatomical structures present around the pancreas including innervation and the difficulty of achieving a “point-by-point” correlation between the imaging and pathological findings. Therefore, no description of PLX invasion is provided in the Union Internationale Contra le Cancer (UICC) classification [22]. However, PhC frequently invades the PLX [13] and the postoperative survival rate for patients with PLX invasion is worse compared with that for patients without PLX invasion [5-12]. Because of this, the Japan Pancreas Society classification [23] adopted the item of PLX invasion and is now considered to be a more reliable staging system predicting the outcome

compared with that based on the UICC classification [24]. Therefore, we consider that the preoperative imaging diagnosis of PLX invasion in PhC is clinically important.

In this study, to make a point-by-point imaging-pathological correlation possible, we cut the en bloc specimens of PhC horizontally, and made double oblique MPR images that were exactly equal to each of the pathological sections. As a result of this correlation analysis, we derived four different CT patterns from the view point of PLX invasion, namely, fine reticular and linear, coarse reticular, mass and strand and nodular patterns. In 92% of the regions investigated showing the mass and strand pattern and 63% showing the coarse reticular pattern (all continuous with PhC), PLX invasion was revealed pathologically, and they were highly suggestive of PLX invasion by PhC on MDCT images ($p < 0.001$). In addition, the blind assessment by independent radiologists confirmed the extremely high diagnostic accuracy of these MDCT patterns.

Concerning the innervation of the pancreas, Yoshioka and Wakabayashi, and Yi et al described that PLX could be divided into two parts [20; 21], “pancreaticus capitalis 1 and 2” as shown in Fig. 1. Yi et al also reported that a few nerves were observed with some small blood vessels and lymphatic vessels diverging complexly with copious connective tissue between the SMA and uncinate process. Our study

confirmed this pancreatic nerve supply pathologically. However, no data are available that suggest that invasion of different parts of the nerve plexus carries different prognostic implications. In addition, it was difficult to differentiate the respective parts of nerve plexuses exactly on the MDCT images because of the intertwined complexity of the PLX. Thus, we determined invasion of the PLX without distinguishing which specific part of the PLX was invaded.

Tian et al and Zhang et al using CT and MRI, respectively, reported that PLX invasion of “pancreaticus capitalis 2” was characterised by streaky and strand-like attenuation or signal intensity structure in fat tissue, and irregular masses adjacent to the tumour [18; 19]. These descriptions correspond approximately to the “mass and strand pattern” in our results. However, in our study, the MDCT criteria of the PLX invasion of any part of the PLX (not only the “pancreaticus capitalis 2”) were not only “mass and strand pattern” but also “coarse reticular pattern” continuous with PhC on MDCT images. That is to say, the criteria of the PLX invasion should be further expanded compared with those previously reported.

Previous reports analysing the imaging findings of PLX invasion did not refer to those of normal structures between the SMA and uncinate process at all. Descriptions of these normal structures were limited to “fat” in previous reports. However, as described above,

there are copious connective tissues with small blood vessels and lymphatic vessels diverging complexly between the SMA and uncinate process pathologically. To know the imaging findings of these normal structures is important for the differential diagnosis of PLX invasion. Based on our results, on MDCT images, there are fine reticular and linear patterns and nodular patterns, and the areas showing these patterns correspond to structures complexly intertwined with micro-vessels, fibrosis, and lymph nodes pathologically. PLX not invaded by tumour is also included in these structures, but it was impossible to distinguish the nerve fibres of PLX from other anatomical structures on MDCT images.

In the areas showing a coarse reticular pattern without PLX invasion, there was a relatively large amount of fibrosis compared with that shown in the areas demonstrating a fine reticular pattern. In addition, two of them showed inflammatory cell infiltration pathologically. Such fibrosis and inflammatory cell infiltration might be caused by tumour-induced chronic pancreatitis complicating PhC, resulting in a major false positive finding for the diagnosis of PLX invasion.

Megibow et al reported that a “thickened vessels sign” surrounding the coeliac axis or SMA associated with pancreatic carcinoma was caused by lymphatic invasion, but without a

“point-by-point” comparison with pathological examination [25]. In the present study, lymphatics were observed pathologically but were likely not to be visualised separately on MDCT images because of their small size compared with micro-vessels or fibrosis. In this study, even when numerous tumour cells were present in this region, PLX invasion was commonly detected but lymphatic invasion was not. All areas showing a nodular pattern were lymph nodes pathologically and were unrelated to PLX invasion.

This study has several limitations. First, it was retrospective in nature and included a relatively small number of patients. To assess the clinical usefulness of PLX invasion on the basis of these CT patterns in individual patients, further prospective study is required. Second, this study did not cover all PLX around the pancreas head. Third, we did not evaluate any cases with chronic pancreatitis or other conditions in the absence of pancreatic cancer. Chronic pancreatitis may also cause a coarse reticular pattern similar to that of PLX invasion.

In conclusion, in the region of the medial-posterior fat area of the pancreas head, ***mass and strand patterns and coarse reticular patterns continuous with PhC on MDCT images were highly suggestive of PLX invasion by PhC.*** These results may help to predict the prognosis of the disease and to decide the surgical strategy including extended resection with surrounding major vessels.

References

1 Matsuno S, Egawa S, Fukuyama S, et al. (2004) Pancreatic Cancer Registry in Japan: 20 years of experience. Pancreas, 28(3):219-230. http://ovidsp.tx.ovid.com/spb/ovidweb.cgi?QS2=434f4e1a73d37e8c01e9bb09ab15b392cdde409bdae0da8d7a43048278daa6de3c938745e122f15ea370ee7099ea5f58990821e88c34c5c220f7fd261b054ce9edb6ee20efc8159053487e23e33c4ea182f66058cfd7c46a878f8fbc8e78840770831ba56cc88f52b2fb27252871e2fa2f596fd1ffc1df57caa3062c2b7a0c224c1a6de28619ab31e1258fc774eaee35f69ef8f695a3fc8c55f77f906156480753a8c6c6b51b17b5b27c37f6109c62cef082514785a92fa686d506aa01ffe06869ff19a98f976d7faad845108b94a682451e6452cc82b02d948d08ed64d2ec9c6329ce9b154dba797ec3b9cbf626a93362f14ea64cbf5737. Accessed 23 Oct 2008

2 Jemal A, Siegel R, Ward E, et al. (2008) Cancer statistics, 2008. CA Cancer J Clin, 58(2):71-96. doi: 10.3322/CA.2007.0010

3 Schnelldorfer T, Ware AL, Sarr MG, et al. (2008) Long-term survival after pancreatoduodenectomy for pancreatic adenocarcinoma: is cure possible? Ann Surg 247(3):456-462. doi: 10.1097/SLA.0b013e3181613142

4 Yekebas EF, Bogoevski D, Cataldegirmen G, et al. (2008) En bloc

vascular resection for locally advanced pancreatic malignancies infiltrating major blood vessels: perioperative outcome and long-term survival in 136 patients. Ann Surg 247(2):300-309. doi: 10.1097/SLA.0b013e31815aab22

5 Kayahara M, Nagakawa T, Konishi I, Ueno K, Ohta T, Miyazaki I (1991) Clinicopathological study of pancreatic carcinoma with particular reference to the invasion of the extrapancreatic neural plexus. Int J Pancreatol, 10(2):105-111.

6 Nagakawa T, Kayahara M, Ueno K, Ohta T, Konishi I, Miyazaki I (1992) Clinicopathological study on neural invasion to the extrapancreatic nerve plexus in pancreatic cancer. Hepato-gastroenterology, 39(1):51-55.

7 Nagakawa T, Kayahara M, Ueno K, et al. (1992) A clinicopathologic study on neural invasion in cancer of the pancreatic head. Cancer, 69(4):930-935. doi: 10.1002/1097-0142(19920215)69:4<930::AID-CNCR2820690416>3.0.CO;2-R

8 Nagakawa T, Mori K, Nakano T, et al. (1993) Perineural invasion of carcinoma of the pancreas and biliary tract. Br J Surg 80(5):619-621. doi: 10.1002/bjs.1800800526

9 Kayahara M, Nagakawa T, Ueno K, Ohta T, Tsukioka Y, Miyazaki I (1995) Surgical strategy for carcinoma of the

pancreas head area based on clinicopathologic analysis of nodal involvement and plexus invasion. Surgery, 117(6):616-623.

10 Nakao A, Harada A, Nonami T, Kaneko T, Takagi H (1996) Clinical significance of carcinoma invasion of the extrapancreatic nerve plexus in pancreatic cancer. Pancreas, 12(4):357-361. http://ovidsp.tx.ovid.com/spb/ovidweb.cgi?WebLinkFrameset=1&S=AOJHFPEHMCDDNECJNCFLCHJLAJJMAA00&returnUrl=http%3a%2f%2fovidsp.tx.ovid.com%2fspb%2fovidweb.cgi%3fMain%2bSearch%2bPage%3d1%26S%3dAOJHFPEHMCDDNECJNCFLCHJLAJJMAA00&directlink=http%3a%2f%2fgraphics.tx.ovid.com%2fovftpdfs%2fFPDDNCJLCHCJMC00%2ffs047%2fovft%2flive%2fgv031%2f00006676%2f00006676-199605000-00006.pdf&filename=Clinical+Significance+of+Carcinoma+Invasion+of+the+Extrapancreatic+Nerve+Plexus+in+Pancreatic+Cancer. Accessed 24 Jul 2008

11 Nakao A, Takeda S, Sakai M, et al. (2004) Extended radical resection versus standard resection for pancreatic cancer: the rationale for extended radical resection. Pancreas, 28(3):289-292. http://ovidsp.tx.ovid.com/spb/ovidweb.cgi?QS2=434f4e1a73d37e8c01e9bb09ab15b39201d3938fc4fac7641a313376699844a0df83d70dbae5acf04dc1f708da9a61d665b10e12fc67128294eeb189b3

4e7e149e5e3ba3db4b5be0549c35e2e1bef651820d842ec6aa613e
d1210f4cfc47c322563572d3907f80b140c6a4595ffe74cbc12457d
741067426659c902779dffb4885b87c44a3a31d8ce5bc7e14a7c80
3ecf9f589e081094e298481a1e5dcc590cf6259e3061c671de69291
1c277e5c97536dfde8891a9addc12aa37f3563bd07df6569d7ef1bc
ac391210af3c5a55ff8f84aff07a1a529775ee1d4de759f102e38a45
ddb4a1c4aa4e6b5d0cbbc9e4fd22a. Accessed 16 Oct 2008

12 Mitsunaga S, Hasebe T, Kinoshita T, et al. (2007) Detail histologic analysis of nerve plexus invasion in invasive ductal carcinoma of the pancreas and its prognostic impact. Am J Surg Pathol 31(11):1636-1644. doi: 10.1097/PAS.0b013e318065bfe6

13 Noto M, Miwa K, Kitagawa H, et al. (2005) Pancreas head carcinoma: frequency of invasion to soft tissue adherent to the superior mesenteric artery. Am J Surg Pathol 29(8):1056-1061. http://ovidsp.tx.ovid.com/spb/ovidweb.cgi?QS2=434f4e1a73d37
e8c3511ef48f69b7c81718b3f5a9e050c86d9d8590bb5736c913e3
673be9b31519e92f0ec8ad2cf3b2e2e791e4e835c912e6b3ab85a24
ab018c6c8d9f120b7b4aa249a7c65864a291d9c8a6157614fb06ac
d9bbae7e7c779759e876da7065b84514dfbdd22bc4f1d03dfd4cd2
4677b7f4a8697e6f029ed8e4218078f7b8d403caff3f7a682959b89
c2fade0c6d994fa96cd131d862ec27159156aac007984d077d5706
471a7a7dcf846615c4c7fb3a1488406906feb05097c9edaf3a08561

3e43bf64f27a78c990169ea5c1be85b1b73cbd27a61eb000913605a70fe5aea5a12e4b8b3063b9695dbb00715541ca9cbcdf4e. Accessed 31 Jul 2008

14 Kato K, Yamada S, Sugimoto H, et al. (2009) Prognostic factors for survival after extended pancreatectomy for pancreatic head cancer: influence of resection margin status on survival. Pancreas, 38(6):605-612. doi: 10.1097/MPA.0b013e3181a4891d

15 Makino I, Kitagawa H, Ohta T, et al. (2008) Nerve Plexus Invasion in Pancreatic Cancer: Spread Patters on Histopathologic and Embryological Analyses. Pancreas, 37(4):358-65. doi: 10.1097/MPA.0b013e31818166e6

16 Miura K (1991) The evaluation of thin slice incremental CE-CT for diagnosis of extension of pancreatic carcinoma--comparison of CT and pathological findings Nihon Igaku Hoshasen Gakkai zasshi, 51(3):245-259. (in Japanese)

17 Demachi H, Hukui N, Miyata S, et al. (1992) CT Findings of Neural Invasion of Nerve plexus Around the Superior Mesenteric Artery in patients with Pancreatic Ductal Carcinoma. Jpn J Clin Radiol, 37:1469-1475. (in Japanese)

18 Tian H, Mori H, Matsumoto S, et al. (2007) Extrapancreatic neural plexus invasion by carcinomas of the pancreatic head region: evaluation using thin-section helical CT. Radiat Med

25(4):141-147. doi: 10.1007/s11604-006-0115-1

19 Zhang XM, Mitchell DG, Witkiewicz A, Verma S, Bergin D (2008) Extrapancreatic neural plexus invasion by pancreatic carcinoma: characteristics on magnetic resonance imaging. Abdom Imaging. doi: 10.1007/s00261-008-9440-4

20 Yoshioka H, Wakabayashi T (1958) Therapeutic neurotomy on head of pancreas for relief of pain due to chronic pancreatitis; a new technical procedure and its results. AMA Arch Surg 76(4):546-554.

21 Yi SQ, Miwa K, Ohta T, et al. (2003) Innervation of the pancreas from the perspective of perineural invasion of pancreatic cancer. Pancreas, 27(3):225-229. http://ovidsp.tx.ovid.com/spb/ovidweb.cgi?QS2=434f4e1a73d37e8c54ea12160ae198c5304aed6a34a11de0b0441ef677e5dfa0065dee75c43bfb4d0d7469c3259437a1427116f4b98b3665068662445053559e27a0f5ee8d1ebe5163bb39d7b7790ea29c0358d67755dab548bec826562abda0570adc3e46208088e1c70788ef931aebf8bb2fd7305d96698303361772d056318146396f9d35ac6e7e9eb5097afed8e24cf55fdcf0cdc1fd0647e8fe48c25dca4743d76808573709ca592bee9b64fb0a903f0769bc65bb4604d1ff63e34e6e66e59092a2de247caaacbece25e3f55728202a46cd7d48b05e06b5fef94366eb3d9760b660cc1a3e95. Accessed 16 Oct 2008

22 Sobin LH, Wittekind C (2002) UICC-TNM classification of malignant tumours, 6th ed. Wiley-Liss, New York,

23 (2003) Japan Pancreas Society. Classification of pancreatic carcinoma, 2nd English ed. Kanehara, Tokyo

24 Isaji S, Kawarada Y, Uemoto S (2004) Classification of pancreatic cancer: comparison of Japanese and UICC classifications. Pancreas, 28(3):231-234. http://ovidsp.tx.ovid.com/spb/ovidweb.cgi?QS2=434f4e1a73d37e8c04d9a87dbb6879060aa0dcfa0542074fe2e8cef0683b49bf51be13f240c5390e3789ddc7160aa6de105053023cb04e20a13e2d204e7baafad99dfcecba4986891d594cfe69df79c8ba8869e6c44abdbd351136c0a5d59b7f7f54278da5ec51439099e58feed35f63f07e710bbb45bb918ac79bf92e6a694125ca55ef9e0af2ec38b635cdd2b894d08dadf66249cbc8537ec4ffba137352e39da7fb0f41f7041d6f431e6c917b783036d065759bae196c9ec2f09a999259a7f7633f38bd69314bd56ba570e283ab1a44000e69b77c6f61e650e597ef89dc7f43731182bf8e14dae0671e41c0f6f13e. Accessed 28 Jul 2008

25 Megibow AJ, Bosniak MA, Ambos MA, Beranbaum ER (1981) Thickening of the celiac axis and/or superior mesenteric artery: a sign of pancreatic carcinoma on computed tomography. Radiology, 141(2):449-453. http://radiology.rsna.org/content/141/2/449.full.pdf+html?sid=90

fe5875-9bf4-41a1-a524-864e0d5edfd0. Accessed 16 Oct 2008

Figure captions

Figure 1

(a) Schema showing the innervation of the pancreas head. PLX are divided into two parts. PLX-1 (= pancreaticus capitalis 1) originates from coeliac ganglions and the coeliac plexus and spreads radically on the posterior surface of the pancreas head and medial margin of the uncinate process. PLX-2 (= pancreaticus capitalis 2) originates from the SMA plexus and spreads on the uncinate process along the IPDA. PLX-1 and 2 interconnect with each other [ref. 20; 21]. (b) Schema of innervation of the pancreas head on two horizontal CT sections. Yellow lines and dots indicate nerve fibres of PLX. Ao = aorta. CA = coeliac artery. CG = coeliac ganglion. CHA = common hepatic artery. DU = duodenum. IPDA = inferior pancreaticoduodenal artery. IVC = inferior vena cava. LRV = left renal vein. P = pancreas. PLX = extrapancreatic nerve plexus. PV = portal vein. SMA = superior mesenteric artery.

Figure 2

(a) The pathological section (H&E, ×1) demonstrates the evaluated structure (arrow). SMA was not resected in this case. (b) Microscopically, a micro-vessel (micro-artery) is identified (arrow) (H&E, ×2). (c) The MPR image produced from a contrast-enhanced CT image adjusted to the pathological section shows a fine line (arrow). Ao = Aorta. CBD = common bile duct. D = duodenum. GDA = gastroduodenal artery. IVC = inferior vena cava. LRV = left renal vein. N = nerve fibres of PLX. PSPDA = posterior superior pancreaticoduodenal artery. PV = portal vein. SMA = superior mesenteric artery. SV = splenic vein. T = primary tumour.

Figure 3

(a) The pathological section (H&E, ×1) demonstrates evaluated structures (white arrow, white arrowhead, black arrow, black arrowhead). One lymph node contains a metastasis (black arrowhead) and the other one is without metastasis (black arrow). CA and SA were not resected in this case. (b) Microscopically, micro-vessels and fibrotic thickenings of adipose tissue septa with PLX (arrowheads) are identified corresponding to the white arrowhead in pathological section (EvG, ×4). There is no PLX invasion by the tumour cells. (c) Microscopically, PLX invasion by the tumour (arrows) with significant fibrosis continuous with PhC identified corresponding to the white arrow on the pathological section (EvG, ×10). (d) The MPR image produced from a contrast-enhanced CT image adjusted to the pathological section shows coarse reticula (white arrow), fine reticula (white arrowhead), mass and strand-shaped soft tissue (black arrow), and nodule (black arrowhead). Ao = Aorta. CA = coeliac artery. D = duodenum. IVC = inferior vena cava. MV = micro-vessels. N = nerve fibres of the PLX. PV = portal vein. SA = splenic artery. T = primary tumour.

Figure 4

(a) Two consecutive pathological sections (H&E, ×1) demonstrate the evaluated structure continuous with PhC (arrowhead and arrow). CA was not resected in this case. (b) Microscopically, PLX invasion by the tumour (arrows) with significant fibrosis is identified on both pathological sections (H&E, ×10). (c) Two MPR images produced from a contrast-enhanced CT image adjusted to the pathological sections show coarse reticula (arrowhead), mass and strand-shaped soft tissue (arrow). Ao = Aorta. CA = coeliac artery. CBD = common bile duct. D = duodenum. DPA = dorsal pancreatic artery. GDA = gastroduodenal artery. IVC = inferior vena cava. N = nerve

fibres of PLX. PV = portal vein. T = primary tumour.

Figure 5

(a) The pathological section (H&E, ×1) demonstrates the evaluated structure (arrow). (b) Microscopically, micro-vessels with fibrotic thickenings of adipose tissue septa with PLX are identified (arrows) (EvG, x4). There is no PLX invasion by the tumour cells. (c) Microscopically, insular lymphocytic infiltrations are also identified (H&E, ×20). (d) The MPR image produced from a contrast-enhanced CT image adjusted to the pathological section shows coarse reticula (arrow). Ao = Aorta. D = duodenum. GDA = gastroduodenal artery. IVC = inferior vena cava. LN = lymph nodes. LRV = left renal vein. N = nerve fibres of the PLX. SMA = superior mesenteric artery. SMV = superior mesenteric vein. T = primary tumour.

Figure 6

Summaries of the four CT patterns. Top: schemas. Bottom: contrast-enhanced CT images corresponding to respective schemas. (a) Fine reticular and linear pattern (arrow) (b) Coarse reticular pattern (arrow) (c) Mass and Strand pattern (arrows) (d) Nodular pattern (arrows).

Figure 7

(a) The Double oblique MPR image produced from a contrast-enhanced CT image adjusted to the pathological specimen shows the area of the fine reticular and linear pattern continuous with PhC (arrow). The primary tumour is not seen on this image. (b) The pathological section (H&E, ×1) demonstrates the corresponding area (arrow). (c) Microscopically, PLX invasion by the tumour cells and minimal fibrosis are

identified in the corresponding area (arrows) (H&E, ×4). Ao = Aorta. D = duodenum. IVC = inferior vena cava. LRV = left renal vein. MVs = micro-vessels. N = nerve fibres of the PLX. SMA = superior mesenteric artery. SMV = superior mesenteric vein.

Table 1. Correlation between the each of the four CT patterns and pathological findings

	Pathological findings		
CT patterns	Complex of micro-vessels/lymphnodes and fibrosis	Lymphnodes	PLX invasion
Fine reticular and linear (n = 113)	112 (99)	0	1 (1)
Coarse reticular (n = 43)	16 (37) *	0	27 (63) †
Mass and Strand (n = 25)	0	2 (8) ‡	23 (92)
Nodular (n = 95)	0	95 (100) §	0

Note. - Data represent the number of the areas showing CT patterns, with percentages to the entire number of CT patterns in parentheses. All cases of PLX invasion were continuous with PhC. PhC = pancreas head carcinoma. PLX = extrapancreatic nerve plexus.

* Seven of them were not continuous and 9 of them were continuous with PhC. Two of them showed inflammatory cell infiltration pathologically.

† All of them were continuous with PhC.

‡ Two of them showed no metastases pathologically.

§ 14 (15%) of them showed metastasis and 81 (85%) of them no metastasis pathologically.

Table 2. MDCT diagnosis and the pathological result of PLX invasion on a patient-by-patient basis

	Pathological result †		
MDCT diagnosis *	+	-	Total
+	25	2	27
-	0	10	10
Total	25	12	37

Note. - Data are the number of the areas showing CT patterns. PLX = extrapancreatic nerve plexus.

* MDCT diagnosis of PLX invasion. + = presence. - = absence.

† Pathological verification of PLX invasion. + = verified. - = not verified.

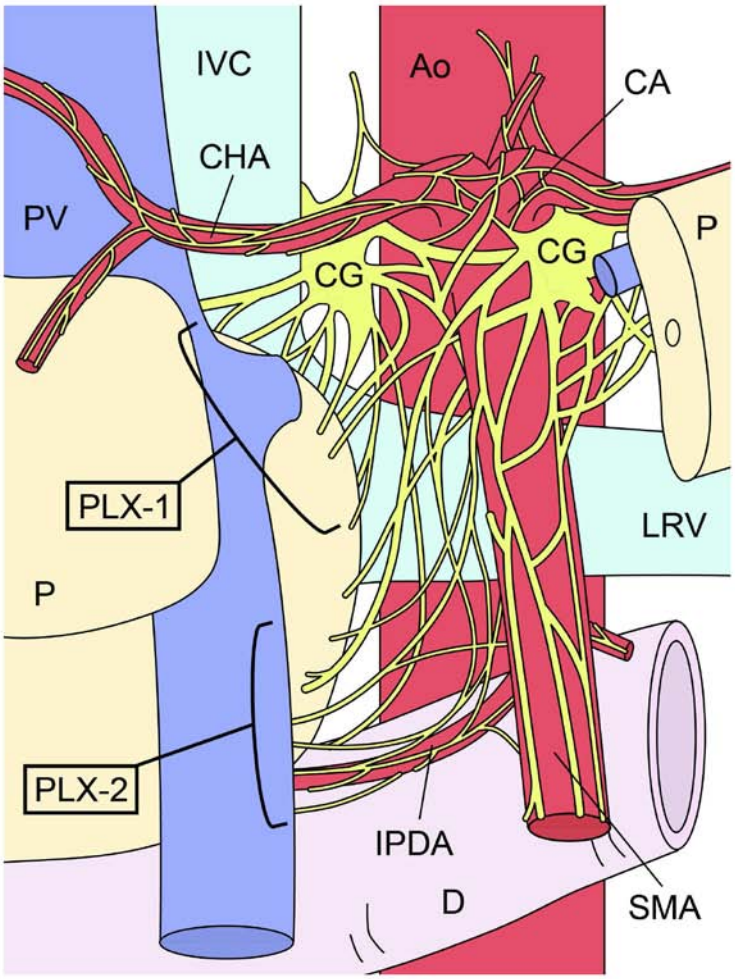

Figure 1 (a):
Schema showing the innervation of the pancreas head. PLX are divided into two parts. PLX-1 (= pancreaticus capitalis 1) originates from coeliac ganglions and the coeliac plexus and spreads radically on the posterior surface of the pancreas head and medial margin of the uncinate process. PLX-2 (= pancreaticus capitalis 2) originates from the SMA plexus and spreads on the uncinate process along the IPDA. PLX-1 and 2 interconnect with each other [ref. 20; 21].
76x101mm (600 x 600 DPI)

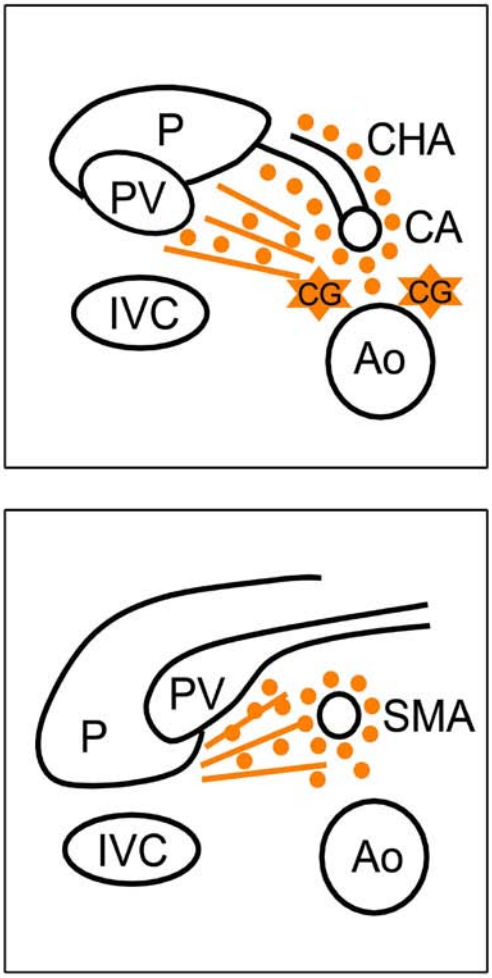

Figure 1 (b):
Schema of innervation of the pancreas head on two horizontal CT sections. Yellow lines and dots indicate nerve fibres of PLX.
76x152mm (600 x 600 DPI)

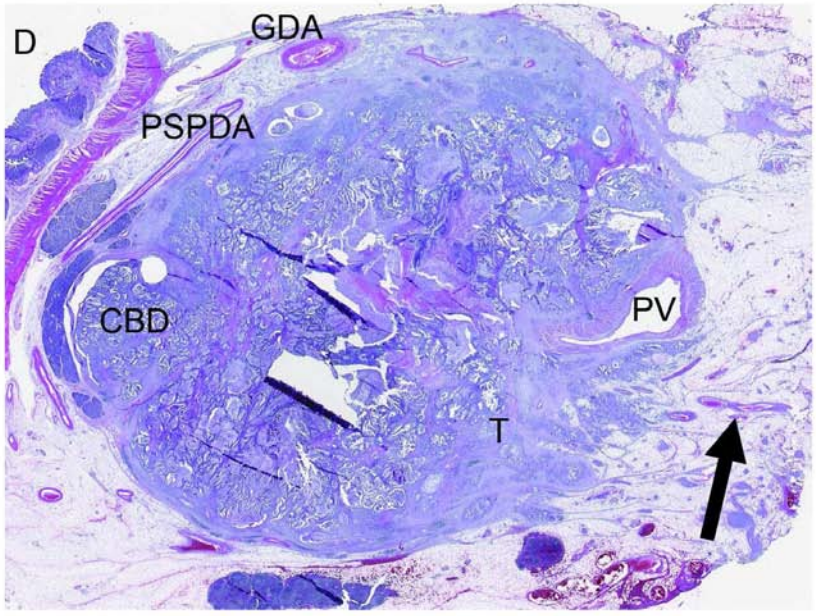

Figure 2 (a):
The pathological section (H&E, ×1) demonstrates the evaluated structure (arrow). SMA was not resected in this case.
101x76mm (300 x 300 DPI)

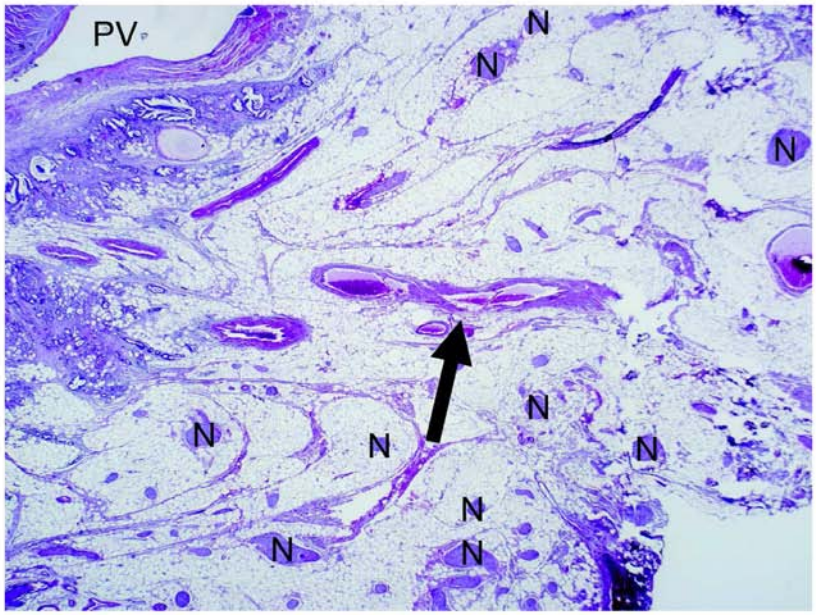

Figure 2 (b):
Microscopically, a micro-vessel (micro-artery) is identified (arrow) (H&E, ×2).
101x76mm (300 x 300 DPI)

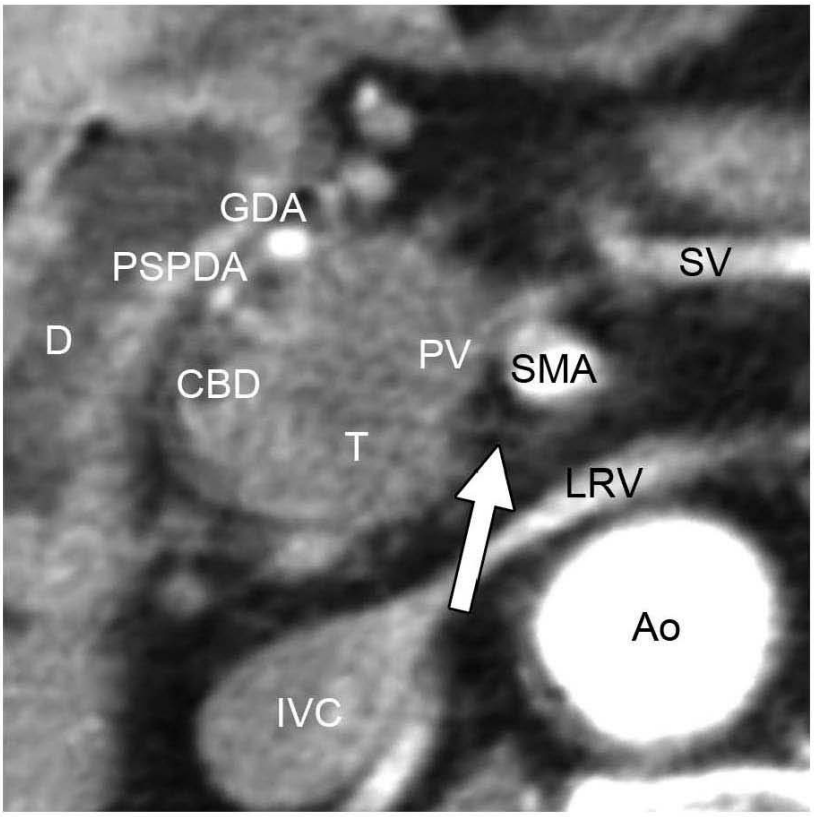

Figure 2 (c):
The MPR image produced from a contrast-enhanced CT image adjusted to the pathological section shows a fine line (arrow).
76x76mm (300 x 300 DPI)

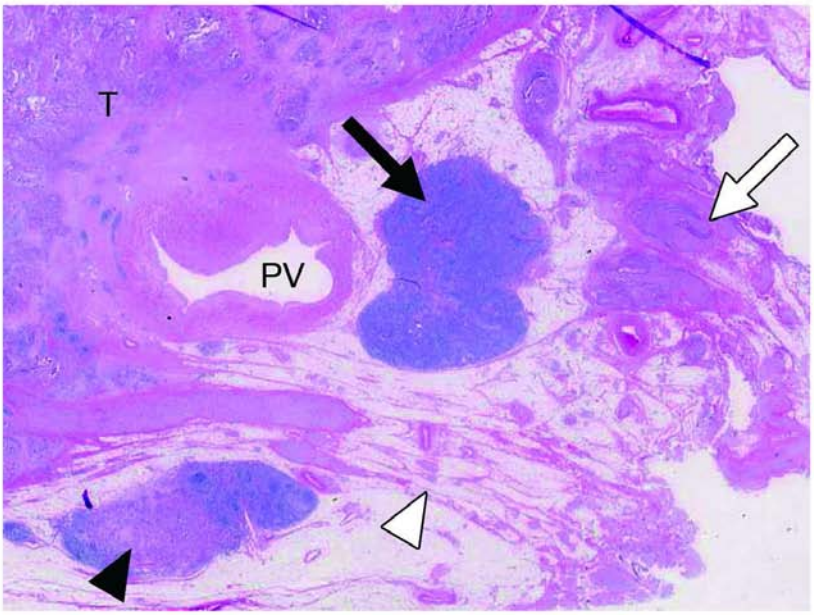

Figure 3 (a):
The pathological section (H&E, ×1) demonstrates evaluated structures (white arrow, white arrowhead, black arrow, black arrowhead). One lymph node contains a metastasis (black arrowhead) and the other one is without metastasis (black arrow). CA and SA were not resected in this case.
101x76mm (300 x 300 DPI)

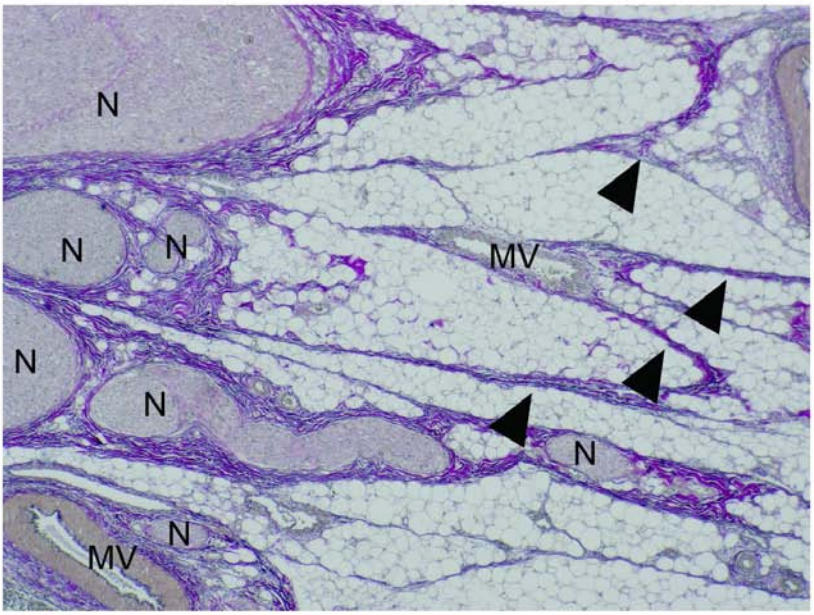

Figure 3 (b):
Microscopically, micro-vessels and fibrotic thickenings of adipose tissue septa with PLX (arrowheads) are identified corresponding to the white arrowhead in pathological section (EvG, ×4). There is no PLX invasion by the tumour cells.
101x76mm (300 x 300 DPI)

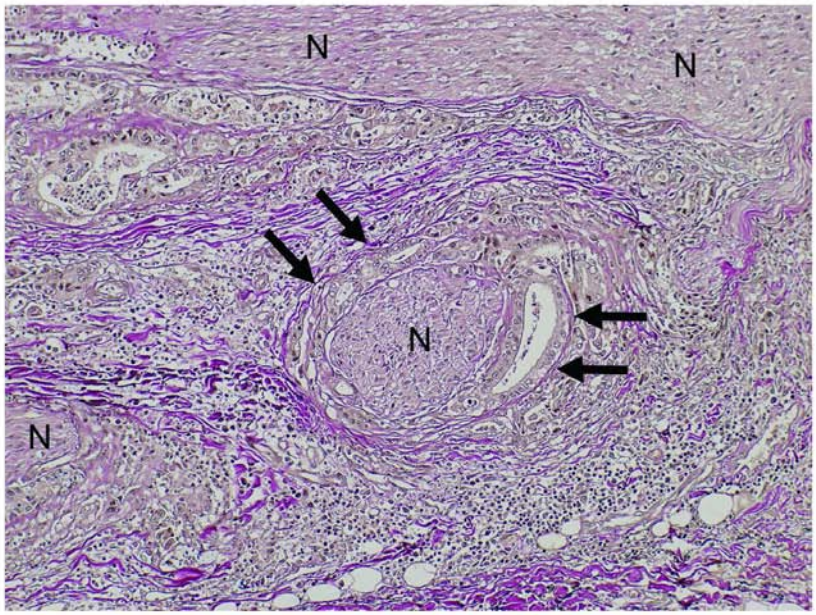

Figure 3 (c):
Microscopically, PLX invasion by the tumour (arrows) with significant fibrosis continuous with PhC identified corresponding to the white arrow on the pathological section (EvG, ×10).
101x76mm (300 x 300 DPI)

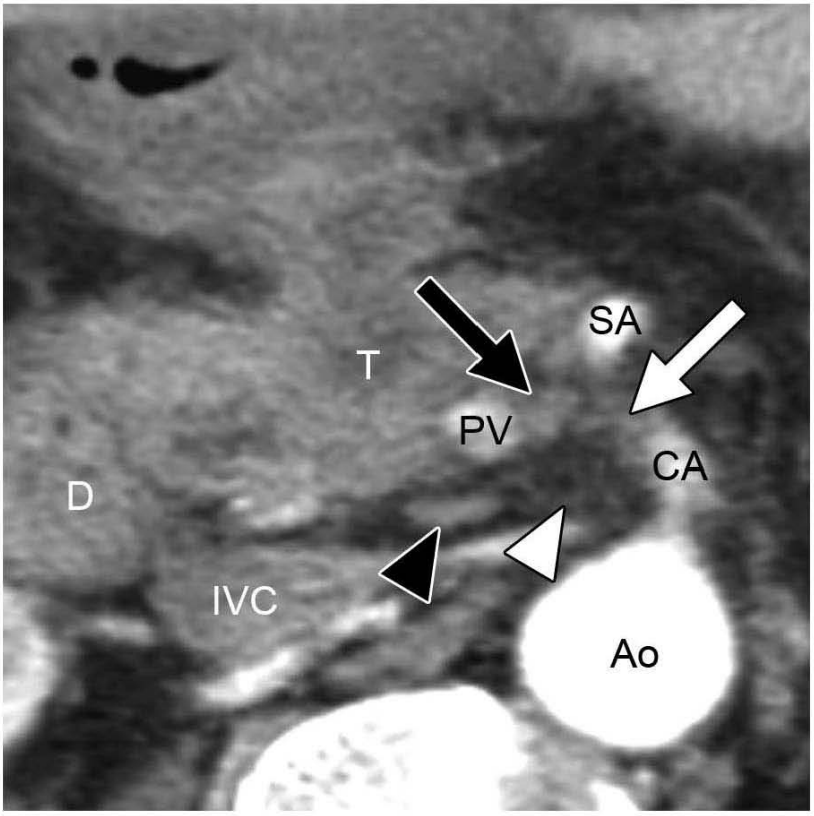

Figure 3 (d):
The MPR image produced from a contrast-enhanced CT image adjusted to the pathological section shows coarse reticula (white arrow), fine reticula (white arrowhead), mass and strand-shaped soft tissue (black arrow), and nodule (black arrowhead).
76x76mm (300 x 300 DPI)

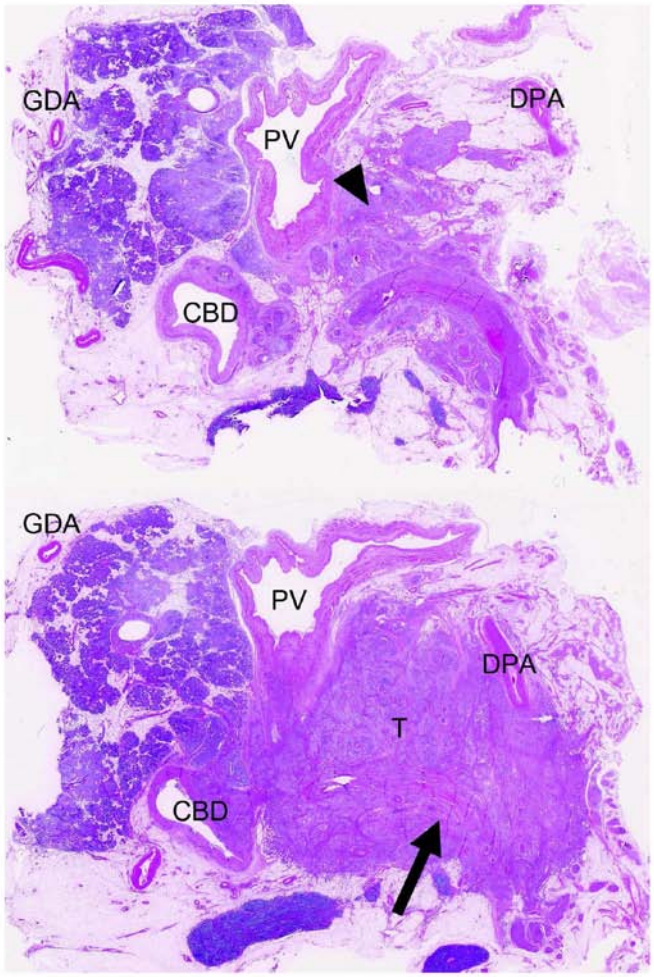

Figure 4 (a):
Two consecutive pathological sections (H&E, ×1) demonstrate the evaluated structure continuous with PhC (arrowhead and arrow). CA was not resected in this case.
101x152mm (300 x 300 DPI)

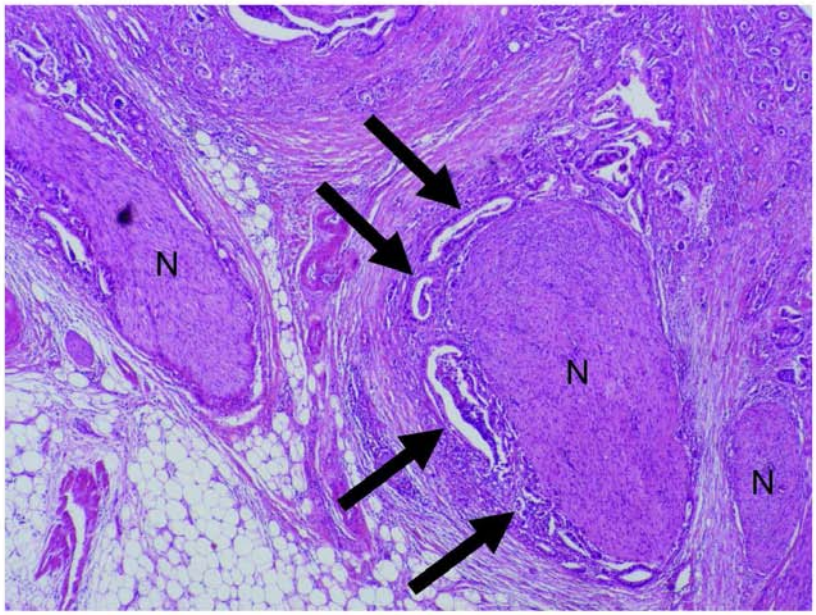

Figure 4 (b):
Microscopically, PLX invasion by the tumour (arrows) with significant fibrosis is identified on both pathological sections (H&E, ×10).
101x76mm (300 x 300 DPI)

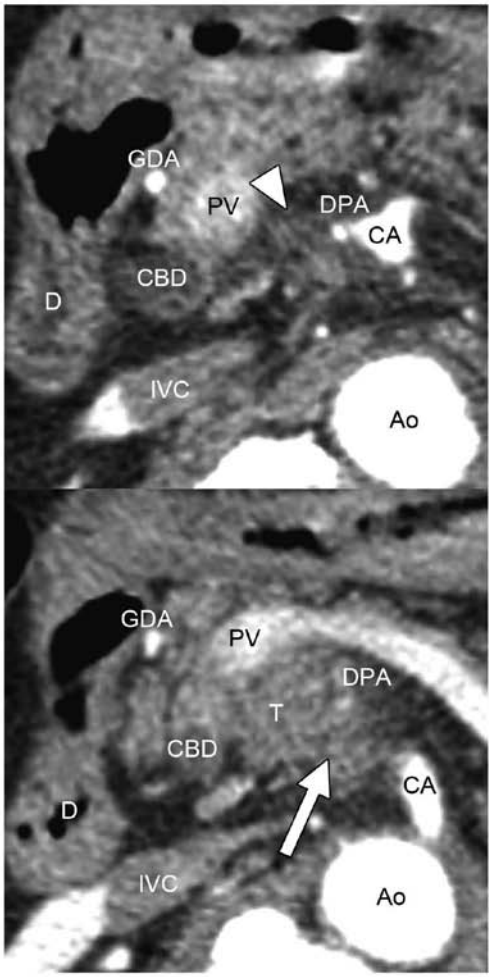

Figure 4 (c):
Two MPR images produced from a contrast-enhanced CT image adjusted to the pathological sections show coarse reticula (arrowhead), mass and strand-shaped soft tissue (arrow).
76x152mm (300 x 300 DPI)

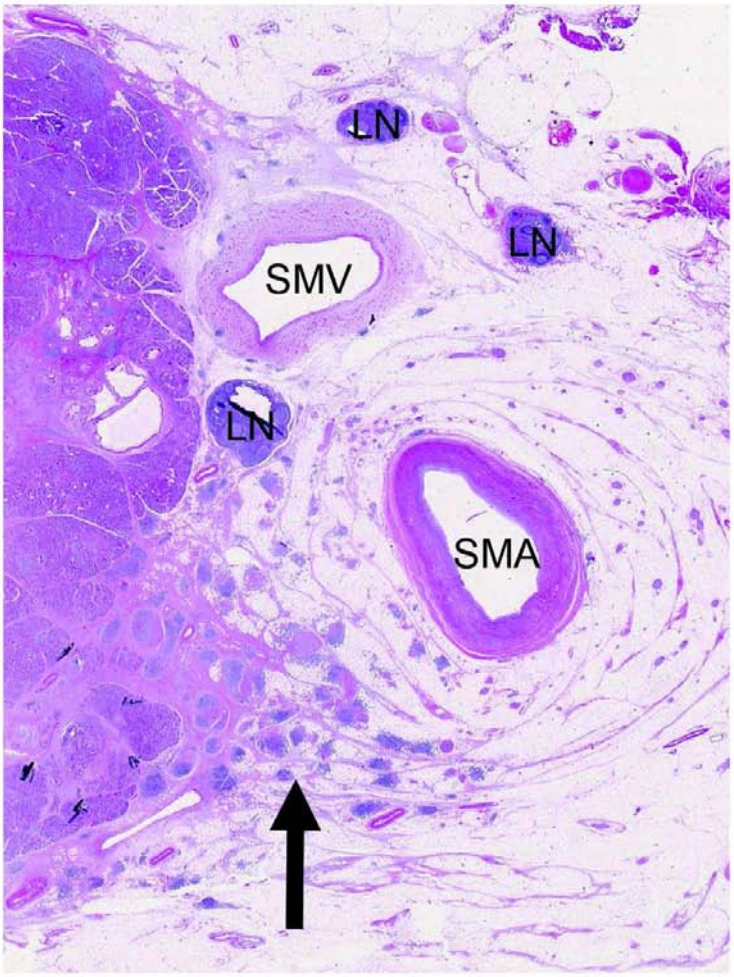

Figure 5 (a):
The pathological section (H&E, ×1) demonstrates the evaluated structure (arrow).
76x101mm (300 x 300 DPI)

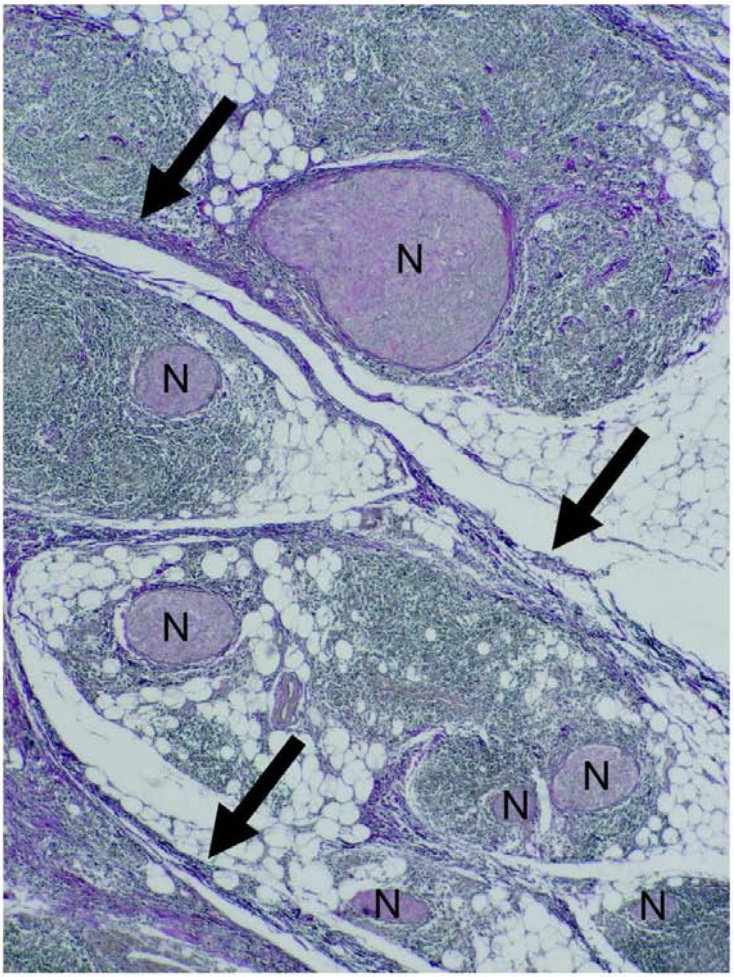

Figure 5 (b):
Microscopically, micro-vessels with fibrotic thickenings of adipose tissue septa with PLX are identified (arrows) (EvG, x4). There is no PLX invasion by the tumour cells.
76x101mm (300 x 300 DPI)

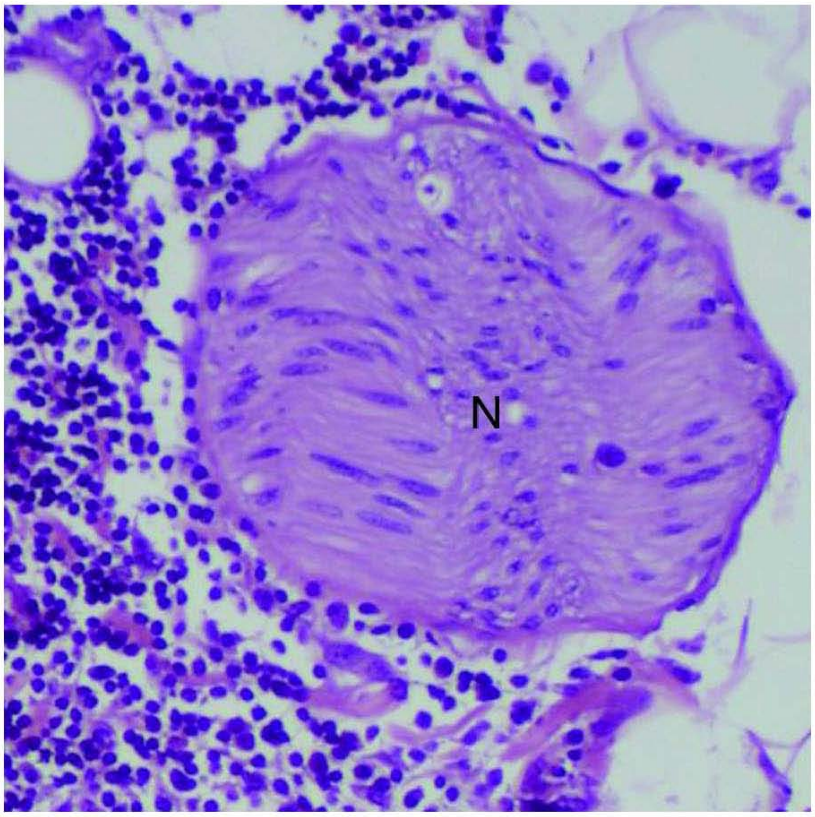

Figure 5 (c):
Microscopically, insular lymphocytic infiltrations are also identified (H&E, ×20).
76x76mm (300 x 300 DPI)

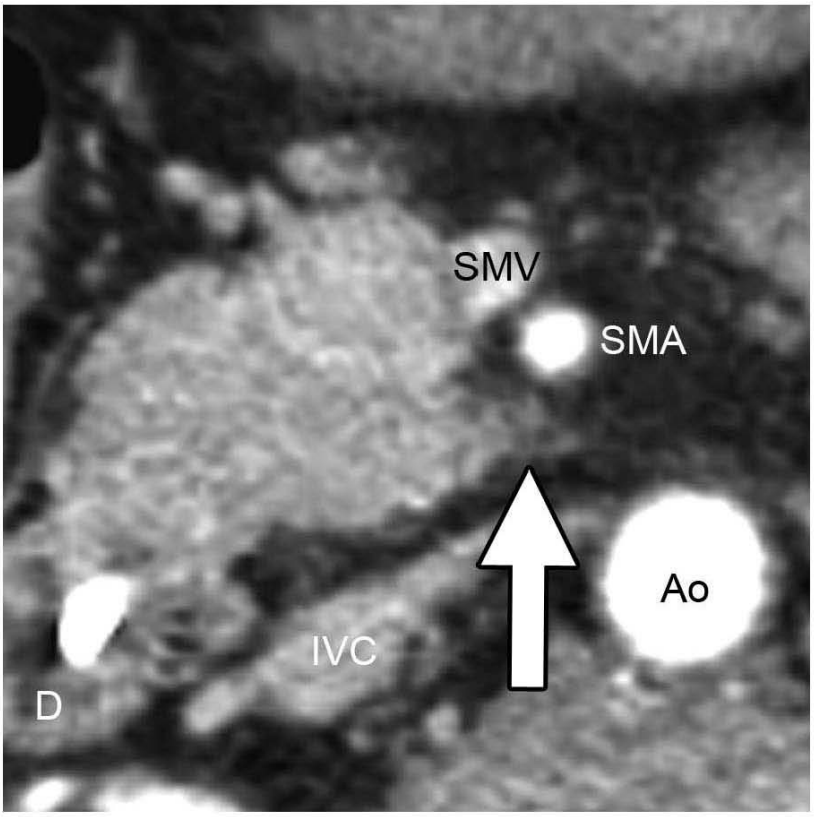

Figure 5 (d):
The MPR image produced from a contrast-enhanced CT image adjusted to the pathological section shows coarse reticula (arrow).
76x76mm (300 x 300 DPI)

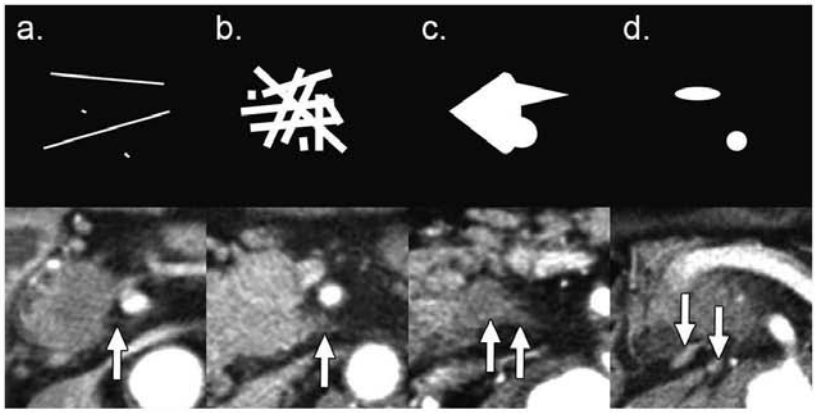

Figure 6:
Summaries of the four CT patterns. Top: schemas. Bottom: contrast-enhanced CT images corresponding to respective schemas. (a) Fine reticular and linear pattern (arrow) (b) Coarse reticular pattern (arrow) (c) Mass and Strand pattern (arrows) (d) Nodular pattern (arrows).
101x50mm (300 x 300 DPI)

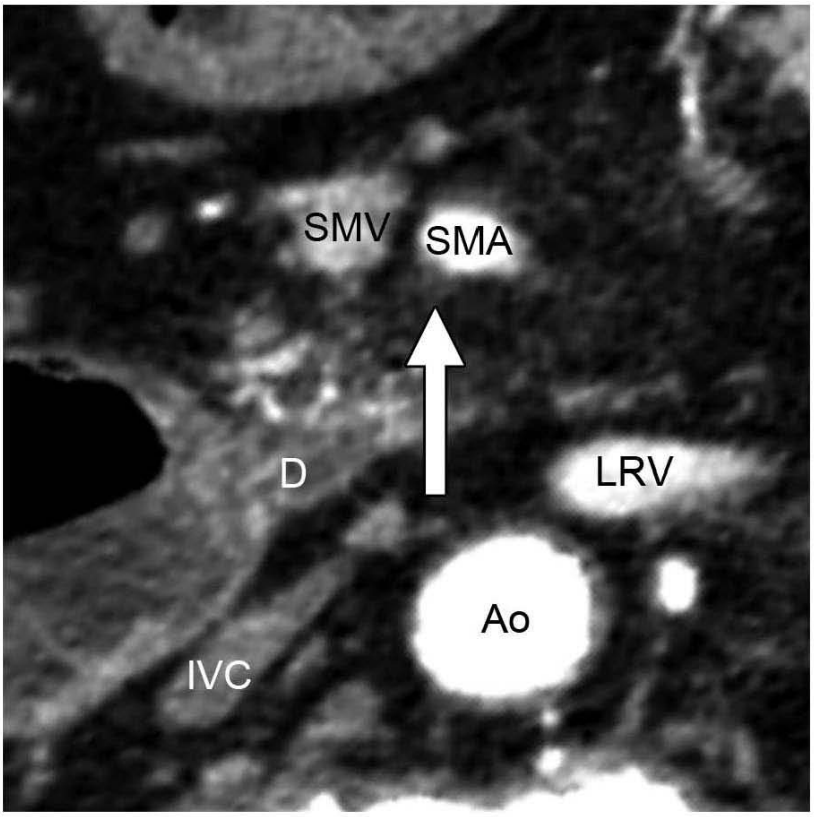

Figure 7 (a):
The Double oblique MPR image produced from a contrast-enhanced CT image adjusted to the pathological specimen shows the area of the fine reticular and linear pattern continuous with PhC (arrow). The primary tumour is not seen on this image.
76x76mm (300 x 300 DPI)

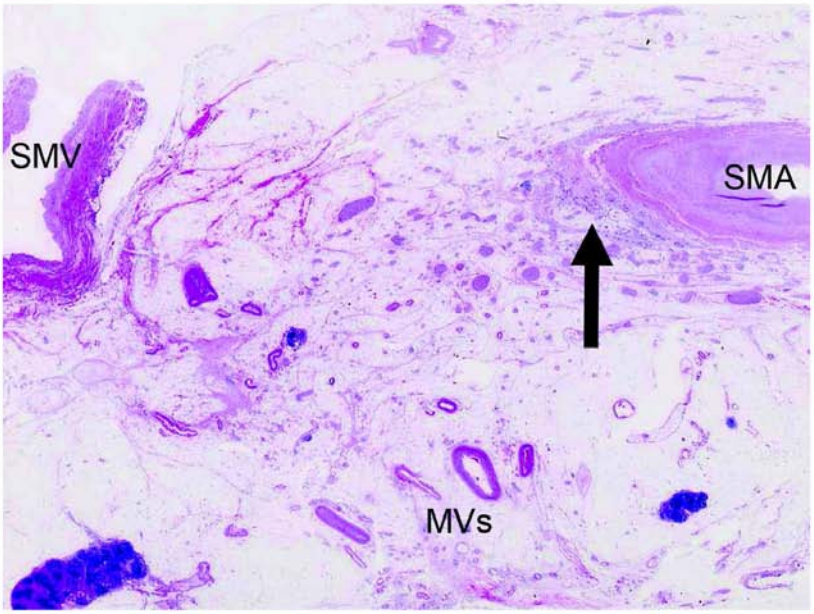

Figure 7 (b):
The pathological section (H&E, ×1) demonstrates the corresponding area (arrow).
101x76mm (300 x 300 DPI)

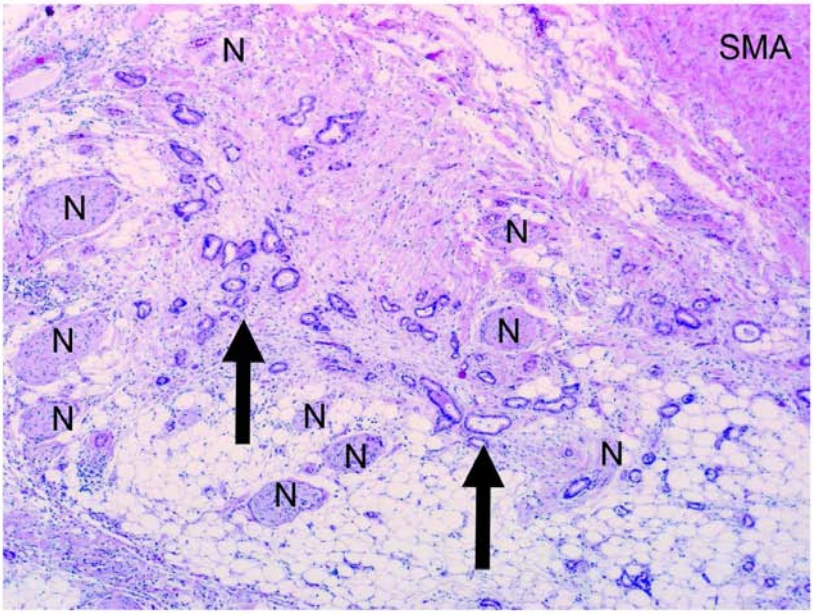

Figure 7 (c):
Microscopically, PLX invasion by the tumour cells and minimal fibrosis are identified in the corresponding area (arrows) (H&E, ×4).
101x76mm (300 x 300 DPI)